CellPress

Cancer Cell
Article

The Risk-Associated Long Noncoding RNA *NBAT-1* Controls Neuroblastoma Progression by Regulating Cell Proliferation and Neuronal Differentiation

Gaurav Kumar Pandey,[1,13] Sanhita Mitra,[1,13] Santhilal Subhash,[1] Falk Hertwig,[9] Meena Kanduri,[7] Kankadeb Mishra,[1] Susanne Fransson,[2] Abiarchana Ganeshram,[1] Tanmoy Mondal,[1] Sashidhar Bandaru,[8] Malin Östensson,[2] Levent M. Akyürek,[8] Jonas Abrahamsson,[5] Susan Pfeifer,[3] Erik Larsson,[8] Leming Shi,[10] Zhiyu Peng,[11,12] Matthias Fischer,[9] Tommy Martinsson,[2] Fredrik Hedborg,[3,6] Per Kogner,[4] and Chandrasekhar Kanduri[1,*]

[1]Department of Medical Genetics, Institute of Biomedicine, Sahlgrenska Academy, University of Gothenburg, 405 30 Gothenburg, Sweden
[2]Department of Clinical Genetics, Institute of Biomedicine, Sahlgrenska Academy, University of Gothenburg, 405 30 Gothenburg, Sweden
[3]Department of Women's and Children's Health, Uppsala University, Uppsala University Hospital, 751 85 Uppsala, Sweden
[4]Department of Women's and Children's Health, Karolinska Institutet, 171 76 Stockholm, Sweden
[5]Department of Pediatrics, The Queen Silvia Children's Hospital, 416 85 Gothenburg, Sweden
[6]Centre for Research and Development, Uppsala University/County Council of Gävleborg, 801 88 Gävle, Sweden
[7]Department of Clinical Chemistry and Transfusion Medicine, Institute of Biomedicine, University of Gothenburg, 405 30 Gothenburg, Sweden
[8]Department of Medical Biochemistry and Cell Biology, Institute of Biomedicine, Sahlgrenska Academy, University of Gothenburg, 405 30 Gothenburg, Sweden
[9]Department of Pediatric Hematology and Oncology, University Children's Hospital of Cologne, and Center for Molecular Medicine Cologne, University of Cologne, 50924 Cologne, Germany
[10]School of Pharmacy, Fudan University, 826 Zhangheng Road, Shanghai 201203, China
[11]BGI-Guangzhou, Guangzhou 510006, China
[12]BGI-Shenzhen, Shenzhen, GuangDong 518083, China
[13]Co-first author
*Correspondence: kanduri.chandrasekhar@gu.se
http://dx.doi.org/10.1016/j.ccell.2014.09.014

SUMMARY

Neuroblastoma is an embryonal tumor of the sympathetic nervous system and the most common extracranial tumor of childhood. By sequencing transcriptomes of low- and high-risk neuroblastomas, we detected differentially expressed annotated and nonannotated long noncoding RNAs (lncRNAs). We identified a lncRNA neuroblastoma associated transcript-1 (*NBAT-1*) as a biomarker significantly predicting clinical outcome of neuroblastoma. CpG methylation and a high-risk neuroblastoma associated SNP on chromosome 6p22 functionally contribute to *NBAT-1* differential expression. Loss of *NBAT-1* increases cellular proliferation and invasion. It controls these processes via epigenetic silencing of target genes. *NBAT-1* loss affects neuronal differentiation through activation of the neuronal-specific transcription factor *NRSF/REST*. Thus, loss of *NBAT-1* contributes to aggressive neuroblastoma by increasing proliferation and impairing differentiation of neuronal precursors.

INTRODUCTION

Neuroblastoma is one of the most common extracranial solid tumors in children. It is thought to arise from improper differentiation of neuronal precursor cells of the sympathetic nervous system. These tumors most commonly occur in the adrenal medulla, but also in sympathetic ganglia of the abdominal organs and of the sympathetic trunk (Brodeur, 2003; Kamijo and Nakagawara,

Significance

Despite recent progress in diagnosis and treatment of neuroblastoma, survival for children with high-risk metastatic neuroblastoma is still less than 50%. This warrants better biological understanding and drug target identification, which could form the basis for improved prognostication, management, and treatment for high-risk neuroblastoma patients. In this study, we identified *NBAT-1 lncRNA* as a prognostic biomarker and potential drug target for therapeutic interventions. Lower expression of *NBAT-1* significantly correlates with poor overall and event free survival probability of neuroblastoma patients. *NBAT-1* controls tumor progression by epigenetically repressing tumor inducing genes and promoting differentiation of undifferentiated tumor cells. Therefore, *NBAT-1* and its target genes may serve as potential targets for drug development and options for high-risk neuroblastoma treatment.

2012). Features like age of the patient at diagnosis, stage of the disease, and nonrandom chromosomal aberrations are well-established parameters for stratification of risk and treatment as well as for predicting the disease outcome in patients (Cohn et al., 2009; Monclair et al., 2009). Neuroblastoma patients with nonrandom chromosomal alterations MNA (*MYCN* amplification)/1p (shorter arm of the chromosome 1) deletion/17q (longer arm of the chromosome 17) gain (seen in 20% of patients) or 11q deletion (11q-) /17q gain (seen in 30% of patients) are often associated with high-risk tumors and an unfavorable outcome. Tumors with hyperdiploidy and numerical aberrations of whole chromosomes are associated with low-risk clinical stages and are prognostically favorable (Brodeur et al., 1984; Carén et al., 2010; Caron, 1995; Guo et al., 1999; Lastowska et al., 2001; Spitz et al., 2003). In addition to nonrandom chromosomal alterations, some neuroblastomas (7%) display recurrent point mutations in the tyrosine kinase domain of the anaplastic lymphoma kinase gene (Carén et al., 2008a; Chen et al., 2008; George et al., 2008; Janoueix-Lerosey et al., 2008; Mossé et al., 2008; Wang et al., 2012a), and genes that take part in neuritogenesis (Molenaar et al., 2012). Recent genome-wide association studies on large patient cohorts have also uncovered clusters of germline SNPs, in six genomic regions. Three SNPs from these clusters map to 6p22 region, and one of the SNPs rs6939340 is located in intronic region of a lncRNA LOC729177. Neuroblastoma patients with homozygous risk G allele at the SNP: rs6939340 are likely to have metastatic disease and poor event free survival (Diskin et al., 2012; Maris et al., 2008). Besides nonrandom somatic genomic alterations and germline SNPs, array based gene expression profiles have also shown associations with clinical subtypes (Fischer et al., 2008).

In the light of current transcriptomic studies, it is evident that the major part of the transcribed genome is noncoding. The RNA from the nonprotein coding genome is mainly comprised of small ncRNAs, long noncoding RNAs (lncRNAs), and unannotated intergenic transcribed regions. LncRNAs have been implicated in diverse cellular processes with distinct regulatory roles (Kanduri, 2011; Whitehead et al., 2009). Several lncRNAs, for example *PCAT-1*, *MALAT1*, *HOTAIR*, and *ANRIL*, have been implicated in tumorigenesis (Batista and Chang, 2013; Prensner and Chinnaiyan, 2011; Prensner et al., 2011; Spizzo et al., 2012; Taft et al., 2010). Thus, studying and evaluating the expression of these nontranslated regions could be of profound value in terms of disease characterization. We therefore set out to identify lncRNA-based biomarkers that could be used in neuroblastoma risk assessment and therapy.

RESULTS

Identification of Transcripts Specific to Distinct Subtypes of Neuroblastomas

In this study, we performed high-throughput transcriptomic profiling of 15 neuroblastoma tumors, three of which were low-risk, whereas of the remaining 12, six each were of the MNA or 11q high-risk subtypes (Carén et al., 2010). An unsupervised clustering analysis on all transcripts detected significant differences in expression signatures between low- and high-risk tumors, as well as between the two subtypes of high-risk tumors (Figures 1A and 1B and Figure S1 available online), indicating that each neuroblastoma subtype carries unique gene expression signatures. We analyzed relative expression of protein coding, annotated and nonannotated lncRNAs by considering the following comparisons of neuroblastoma tumors: low-risk versus 11q-, low-risk versus MNA, low-risk versus high-risk subtypes, and 11q- versus MNA. These comparisons revealed several differentially expressed transcripts (false discovery rate [FDR] < 0.1) (Figures 1C and 1D). We found a significant overlap for protein coding genes between our analysis and the published microarray data set based on expression profile of 88 primary neuroblastoma tumors (R2 database http://r2.amc.nl) (Table S1). We performed pathway analysis on differentially expressed protein coding genes and found eight low-risk specific, 25 11q- specific, and five MNA specific pathways with significant p values from the comparisons between the three subtypes as shown in Figures 1A and S1; Table S2. Mutational screening of genes differentially expressed in this study showed that 27.4% (194/707) carried somatically acquired SNP or insertion and deletion variations predicted to result in nonsilent changes of coding regions, either in our exome sequencing study or previously published neuroblastoma (NBL) sets of 13 and 349 tumors, respectively, (Molenaar et al., 2012; Pugh et al., 2013; Sausen et al., 2013) in comparison to 19.3% (3,787/19,638) of nondifferentially expressed genes. Of the 707 differentially expressed genes, 11 genes (1.56%) (*ALK, MUC4, AHNAK2, AHNAK, DOCK8, FBN2, HSPG2, MYCN, TNC, KIAA0319*, and *ODZ4*) showed a mutation frequency >1% with most recurrent mutations in *ALK*, concordant with previous studies, whereas 61 genes (0.31%) of the nondifferentially expressed showed mutation frequency >1% with most recurrent mutations in *MUC16* (6.6%) and *TTN* (5.8%) (Table S3). However, when we applied the MutSigCV v1.3 algorithm (Lawrence et al., 2013) for all NBL sets, only the differentially expressed *ALK* and the nondifferentially expressed *ZNF717* were found to be significantly mutated. Since the MutSigCV algorithm was developed against tumors with high frequency of mutations, functional significance of rare mutations identified in this study remains to be investigated in pediatric tumors, which are known to harbor few somatic mutations.

The Expression Profile of Nonannotated Long Noncoding RNAs Distinguishes between Low-Risk and High-Risk Neuroblastoma

Differential expression analysis of lncRNAs between low- and high-risk neuroblastomas revealed 24 nonannotated lncRNAs (named as *CUFF* 1–24) (Figure S2A). As can be seen in the heatmap (Figure 2A), the expression profiles of these nonannotated lncRNAs clearly distinguish these two subtypes of tumors. The relative expression of four of these transcripts is depicted in box plots (Figure S2B). We validated their differential expression in an independent cohort of 23 primary neuroblastoma tumors representing low- and high-risk subtypes (Figure 2B). Interestingly, many of these transcripts (9 of the 24) map to the chromosome 6q arm and show significant overexpression in high-risk neuroblastomas compared to the low-risk subset (Figure S2C). The Array comparative genomic hybridization (CGH) profiles of the sequenced tumors did not show any genomic alterations at these transcribed regions.

As lncRNAs are known to be expressed at lower levels in comparison to protein coding transcripts, many lncRNAs tend to filter

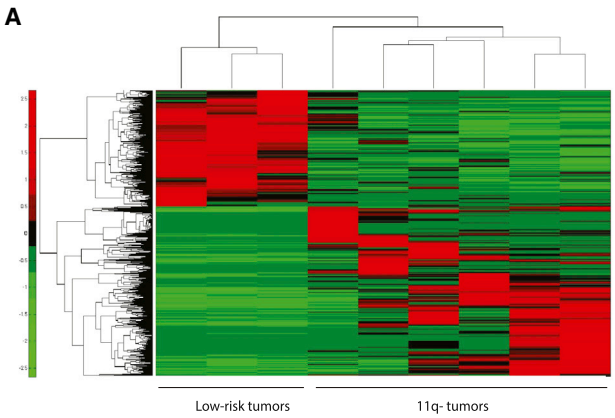

C

Features	Low-risk Vs 11q-	Low-risk Vs MNA	Low-risk Vs High-risk	MNA Vs 11q-
Protein_coding	408	375	43	1066
Non-annotated transcripts	109	255	24	304
Polymorphic_pseudogene	1	4	0	1
antisense	1	0	0	2
lincRNA	7	5	0	8
rRNA_pseudogene	4	8	0	3
processed_transcript	3	7	0	9
pseudogene	15	38	0	5
snoRNA	33	53	3	2
sense_overlapping	0	1	0	3
misc_RNA	1	3	0	1
snRNA	1	4	0	0
miRNA	1	1	0	0
scRNA_pseudogene	0	1	0	0
sense_intronic	0	1	0	0
Total	584	756	70	1404

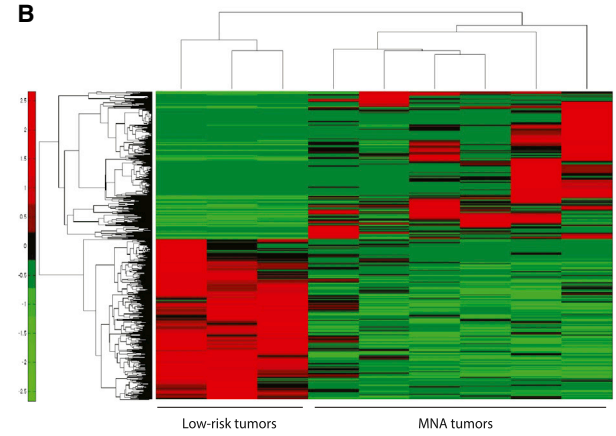

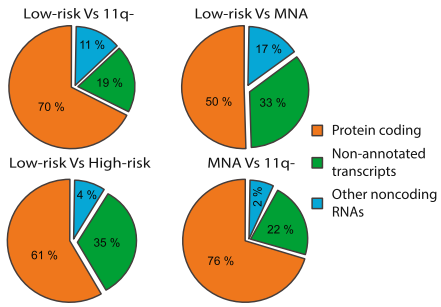

Figure 1. Differential Expression of Transcripts among Three Subtypes of Neuroblastomas

(A and B) Clustergrams (hierarchical clustering) representing the clustering and expression differences among the compared subtypes. Data is represented as euclidean distance metric.

(C) List of differentially expressed transcripts (coding and noncoding) between the four different comparisons among the subtypes of sequenced neuroblastomas.

(D) Pie chart depicting the percentage of different classes of transcripts differentially expressed between low- and high-risk tumors.

See also Figure S1 and Tables S1, S2, and S3.

out in differential expression analysis. Therefore to increase the sensitivity for detecting differentially expressed lncRNAs, we repeated the analyses exclusively on the lncRNA subset. These analyses revealed 325 and 130 differentially expressed lncRNAs between low-risk versus MNA tumors, and low-risk versus 11q- tumors, respectively (Figures S2D and S2E; Table S4). We next investigated whether any of the differentially expressed lncRNAs from low- versus high-risk comparisons map to the characteristic chromosomal abnormalities. We identified a 2 kilobases (kb) lncRNA; mapping to the coamplified region located 293 kb from the *MYCN* locus (Carén et al., 2008b; Schwab, 1998). Similar to *MYCN*, this lncRNA is overexpressed in MNA tumors as compared to the sequenced low-risk and 11q-tumors (Figures 2C, 2D, S2F, and S2G). We observed a similar overexpression of the lncRNA in an independent set of five MNA tumors compared to the low-risk and 11q-tumors (Figure S2G). The hemizygous deletion of the 11q23 arm is another well-known genomic aberration observed in case of non-MNA aggressive tumors (Guo et al., 1999). We detected a lncRNA with significant differential expression mapping to the deleted 11q23 region, showing lower expression in the 11q-tumors compared to the low-risk tumors (Figures 2E, S2H, and S2I). Deletions in the 1p arm are also known to be associated with aggressive neuroblastomas. We identified five additional lncRNAs at the proximal end of the 1p arm with low expression in MNA tumors compared to 11q- and low-risk tumors (Figure 2F). So we are able to provide a putative list of differentially expressed nonannotated and annotated lncRNAs that map to genomic regions that are prone to alterations in high-risk aggressive neuroblastoma tumors.

Neuroblastoma Associated Transcript-1 Is a Potential Marker for Risk Assessment in Neuroblastoma

Our analyses on MNA and low-risk tumors revealed *LOC729177* (GENCODE annotation, also referred to as *CASC14*) lncRNA as one of the top ranked candidates with a significant p value (Table S5; $p = 0.0012$). This transcript also appears as a differentially expressed candidate between low- and high-risk tumors ($p = 0.002$); it is expressed at low level in high-risk tumors compared to low-risk tumors. Because the lncRNA harbors the high-risk associated SNP: rs6939340 in its intron, we were interested in

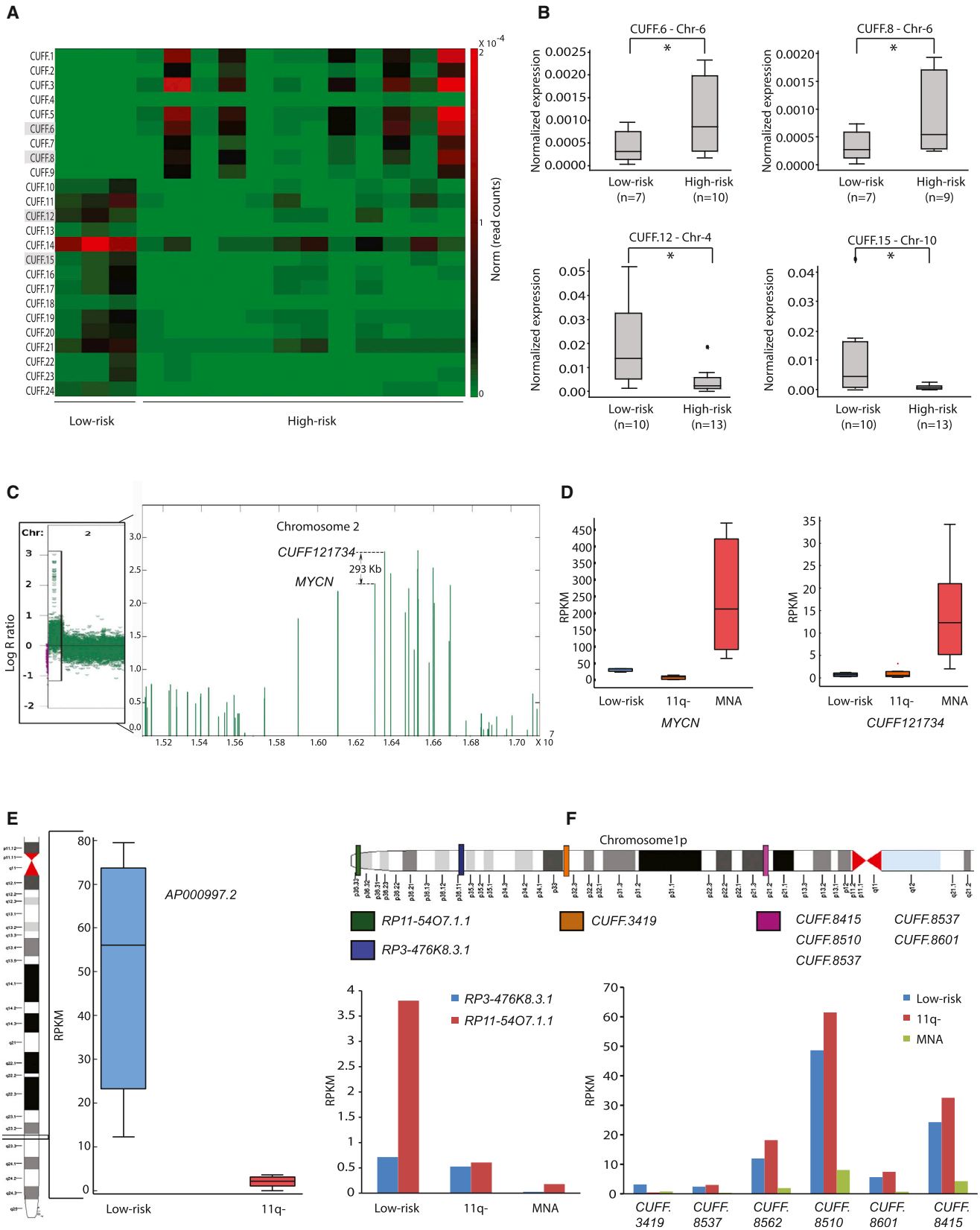

(legend on next page)

understanding the functional connection between the SNP and *LOC729177* and the role of *LOC729177* in neuroblastoma pathogenesis.

Due to its association with neuroblastoma prognosis, we named this RNA as neuroblastoma associated transcript 1 (*NBAT-1*). Using the codon substitution matrix and Coding Potential Assessment Tool (CPAT), as well as a comparison with known protein sequences (Swiss-prot), we have evidence that *NBAT-1* is a noncoding transcript (Figures S3A and S3B) (Wang et al., 2013). The PhastCons score (Pollard et al., 2010) demonstrates that some regions of *NBAT-1* are similar across mammalian species, indicating a possible evolutionarily conserved function (Figure S3C). It has tissue specific expression, mainly in the brain, breast, and ovary (Figure S3D). Consistent with our sequencing data; we observed a significantly lower expression of the *NBAT-1* in high-risk tumors compared to the non high-risk tumors when analyzed in a clinical cohort comprising 93 neuroblastoma patients (Figure 3A). We further validated *NBAT-1* differential expression in RNA sequencing data obtained from an independent clinical cohort of 498 neuroblastomas (Figures 3B, 3C, S3E, and S3F). Analysis of the prognostic value of *NBAT-1* indicated that patients with high *NBAT-1* expression were associated with good prognosis (5 year overall survival [OS] of 0.86 ± 0.02, and 5 year event free survival [EFS] 0.74 ± 0.03) as compared to patients with low *NBAT-1* expression (5 year OS of 0.66 ± 0.04, and 5 year EFS of 0.44 ± 0.04) (Figures 3D–3F and S3G). Furthermore, the waterfall plot for ordered *NBAT-1* expression across all analyzed tumors with patient outcome corroborates the findings from the survival analysis (Figures 3G and S3H). Importantly, the multivariate Cox regression analysis on the independent clinical cohort ($n = 498$, hazard ratio = 0.839, and $p = 0.038$) suggests that *NBAT-1* may act as an independent prognostic marker in predicting event free survival (Figure 3H). In addition, *NBAT-1* could give prognostic information for children with both MNA+ and MNA- tumors (Figures S3I–S3L). This indicates that *NBAT-1* expression is a significant independent prognostic factor that could serve as an additional prognostic marker for risk assessment in neuroblastoma patients.

We next sought to address the functional link between the high-risk neuroblastoma associated SNP: rs6939340 and *NBAT-1* expression in primary tumors. We sequenced genomic DNA over the SNP from 51 high-risk primary tumors used in the quantitative reverse transcription (qRT)-PCR validation. High-risk tumors with either A/G or A/A genotype had higher expression in comparison to tumors with G/G genotype ($p = 0.03$) (Figures 4A and S4A). Thus, G/G genotype might be associated with lower *NBAT-1* expression in high-risk tumors. We next genotyped the SNP and analyzed the *NBAT-1* expression in six neuroblastoma cell lines (Figure 4B). The SK-N-FI cell line with a G/G genotype showed lower *NBAT-1* expression compared to the SH-SY5Y cell line with an A/A genotype. In addition, fragments carrying the SNP generated more luciferase activity in PGL3 promoter vectors, with an A/A genotype showing more luciferase activity than the G/G genotype, indicating that the region spanning the SNP might be a putative enhancer element (Figure 4C). In addition, higher order regulatory interactions between the SNP and *NBAT-1* promoter were detected in a chromosome conformation capture (3C) experiment and in RNA polymerase II chromatin interaction analysis by paired-end tags (PolII ChIA-PET) using the ENCODE data set in MCF7 cells (Li et al., 2012) (Figure 4D). The SNP region also carries characteristic enhancer-specific marks (Figure 4E). The enrichment of enhancer specific marks and 3C interaction was significantly lower in G/G as compared to the A/A genotype (Figures 4D and 4E).

We next investigated additional factors that contribute toward differential *NBAT-1* expression between low- and high-risk neuroblastoma patients by analyzing DNA methylation at CpG nucleotide sites flanking the *NBAT-1* promoter using pyrosequencing. We found that five CpGs flanking the *NBAT-1* promoter were significantly hypermethylated in high-risk patients, with lower *NBAT-1* expression; whereas the CpGs were hypomethylated in low-risk patients with higher *NBAT-1* expression (Figures 4F and S4B–S4F). In addition, significant activation of the *NBAT-1* expression was detected in SK-N-AS cells upon treatment with DNA demethylating agent 5-Aza-2′-deoxycytidine (DAC). These observations together suggest that DNA methylation plays a functional role in the inactivation of the *NBAT-1* promoter in high-risk patients (Figure 4G).

Neuroblastoma Associated Transcript-1 Harbors Tumor Suppressor Properties

Since the lower expression of *NBAT-1* is correlated with aggressiveness in neuroblastoma patient tumors, we investigated the effect of downregulation of *NBAT-1* on the SH-SY5Y cells. Depletion of *NBAT-1* using two siRNAs (si-A and si-C) in the SH-SY5Y cell line resulted in a significant increase in the number of viable cells compared to the cells transfected with control siRNA (Figures 5A and S5A). In addition, we generated a SH-SY5Y cell line stably transduced with lentivirus carrying *NBAT-1* specific short hairpin RNA (NBAT1-sh) that displays a 70% to 80% downregulation of *NBAT-1* compared to the cell line stably transduced with lentivirus containing a scrambled short hairpin

Figure 2. Nonannotated Long Noncoding RNAs Are Differentially Expressed between Low- and High-Risk Tumors

(A) Heatmap depicting the expression differences of nonannotated transcripts (*CUFF*.1–24) between low- and high-risk tumors.

(B) qRT-PCR validation of four differentially expressed *CUFFs* in an independent cohort of neuroblastoma tumors. The expression levels were normalized to corresponding *GAPDH* levels, and the normalized values are presented as boxplots where *n* represents the number of primary tumors used. The p values are presented as obtained from student's t test (two tailed and unequal variance).

(C) Representative CGH Array profile of an amplified region containing *MYCN* on chromosome 2. The lncRNA *CUFF.121734* is shown as coamplified along with the *MYCN* gene.

(D) Normalized read counts (reads per kb of transcript per million reads mapped [RPKM] from sequencing) of *MYCN* and *CUFF.121734* show the differences in expression between the three subtypes.

(E) Genomic region on chromosome arm 11q showing lncRNA *AP000997.2*, differentially expressed between low-risk and 11q- tumors.

(F) P arm of the chromosome 1 depicting the differentially expressed noncoding transcripts between the three subtypes. Bar graphs showing the normalized expression levels (RPKM) of these transcripts between the three subtypes.

For (B), values represent mean ±SD. *$p < 0.05$. See also Figure S2 and Tables S4 and S5.

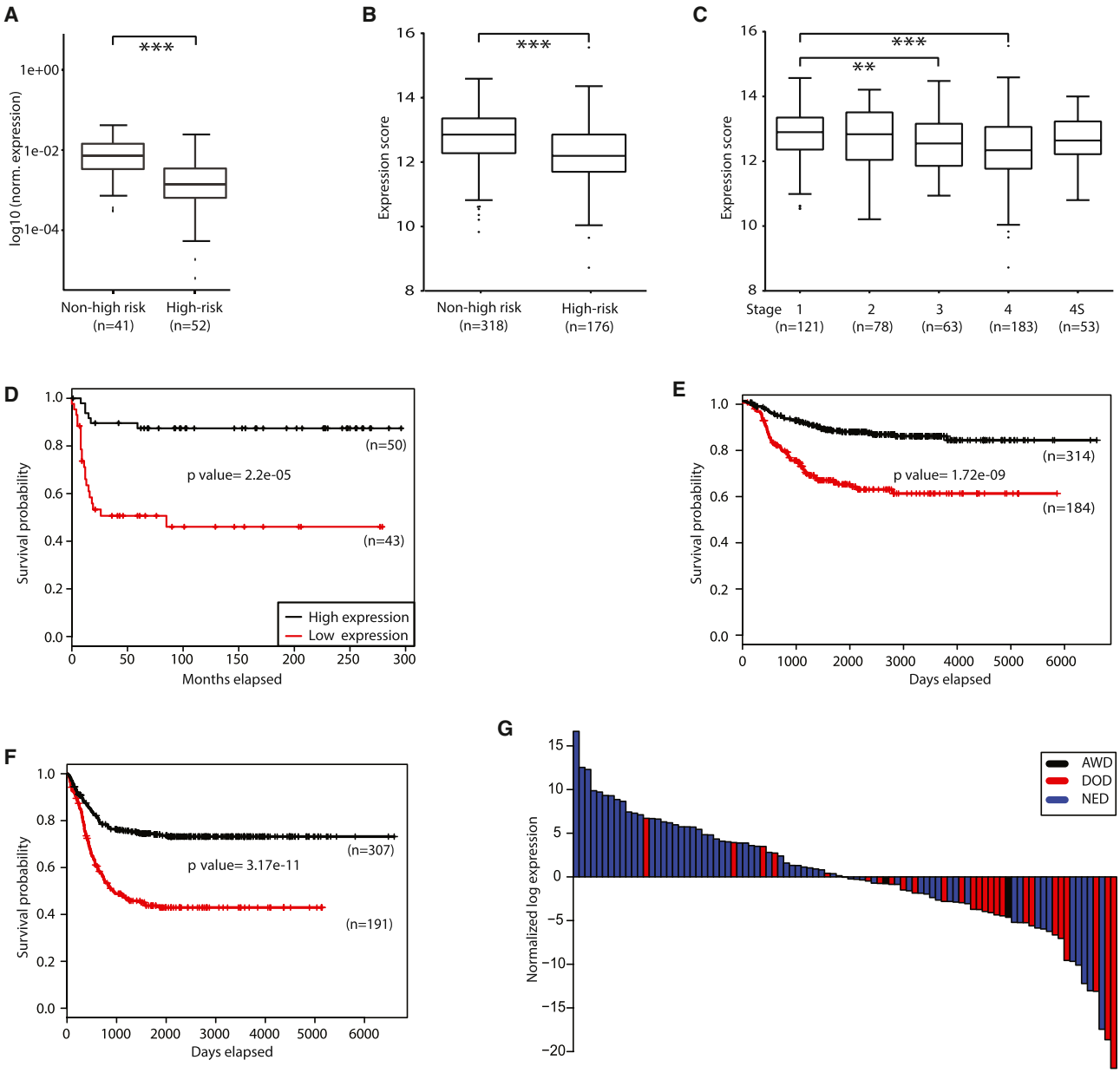

H

Model	n	EFS HR	EFS 95% CI of HR	EFS p-value	OS HR	OS 95% CI of HR	OS p-value
- *NBAT-1* (continous)	493	0.839	[0.711;0.989]	0.038	---	---	0.640
- Age (≥ 18 months vs < 18 months)		1.818	[1.277;2.589]	0.001	3.451	[1.996;5.965]	0.000001
- *MYCN* (amp. vs non amp.)		1.603	[1.122;2.290]	0.010	3.566	[2.372;5.362]	2.0143×10^{-9}
- Stage (4 vs 1-3, 4S)		2.361	[1.653;3.374]	0.000002	3.364	[1.990;5.689]	0.000001
- *NBAT-1* (≥ 12.4 vs <12.4)	493	0.577	[0.415;0.803]	0.001			
- Age (≥ 18 months vs < 18 months)		1.803	[1.269;2.562]	0.001			
- *MYCN* (amp. vs non amp.)		1.463	[1.024;2.089]	0.038			
- Stage (4 vs 1-3, 4S)		2.314	[1.617;3.310]	0.000003			
- *NBAT-1* (≥ 12.3 vs <12.3)	493				---	---	0.867
- Age (≥ 18 months vs < 18 months)					3.451	[1.996;5.965]	0.000001
- *MYCN* (amp. vs non amp.)					3.566	[2.372;5.362]	2.0143×10^{-9}
- Stage (4 vs 1-3, 4S)					3.364	[1.990;5.689]	0.000001

(legend on next page)

RNA (Cntrl-sh) (data not shown). The *NBAT-1* shRNA transduced SH-SY5Y cell line also showed a similar increase in the number of viable cells, further confirming the antiproliferative activity of *NBAT-1* (Figure S5B). Suppression of *NBAT-1* expression also led to increased invasiveness of SH-SY5Y cells (Figure 5B). Consistent with its antiproliferative property, we observed a significant increase in the growth rate of *NBAT-1* depleted xenografts (Figures 5C–5E). Hematoxylin and eosin staining of xenograft sections of the NBAT1-sh and Cntrl-sh xenografts did not reveal any gross morphological abnormalities (Figure 5F). However, using Ki67, a marker for cell proliferation, we observed a significant increase in the number of replicating cells in *NBAT-1* depleted xenografts as compared to control xenografts (Figures 5F and 5G). Together, these findings indicate that *NBAT-1* harbors tumor suppressor properties.

In order to identify the putative targets of *NBAT-1* and to understand its inhibitory role in tumorigenesis, we sequenced the total RNA from NBAT1-sh cells along with Cntrl-sh cells. There were 1,348 (987 upregulated and 361 downregulated) protein-coding genes (2-fold expression difference, FDR of < 0.05) that showed differential expression upon *NBAT-1* downregulation (Figures S5C and S5D; Table S6). Importantly, the neighboring transcript LINC00340 (*CASC15*) was not significantly affected upon *NBAT-1*'s downregulation (data not shown). Gene ontology analysis of the differentially expressed genes showed significant enrichment for biological processes such as cell differentiation, cell migration, and cell proliferation, along with neuronal processes; nervous system development, neurogenesis, and neuron differentiation (FDR < 0.05) (Figure 5H). Given that abnormal cell proliferation and migration are among the important contributing factors underlying tumor initiation and progression, we addressed plausible mechanisms by which *NBAT-1* controls these biological processes. We noted that 49 (out of 335 genes; 15%) cell proliferation-specific genes and 57 genes implicated in cell migration (121 genes; 47%) were among the 1,348 differentially expressed *NBAT-1* target genes (Figures 5I and 5J; Table S6). Differential expression of some of the key target genes was validated upon *NBAT-1* downregulation using sh-RNA and two siRNAs (si-A and si-C) (Figures 5K and S5E), including *VCAN*, *SOX9*, and *OSMR*, which are reported to be overexpressed in a wide range of tumors (Cheon et al., 2014; Kopp et al., 2012; Matheu et al., 2012; West et al., 2012; Yeung et al., 2013). Interestingly, when the gene expression changes after *NBAT-1* downregulation were compared with the R2 data set (comprising differential expression of protein coding genes between low- and high-risk tumors), 45 common candidate genes were found to have similar expression profiles, including *VCAN* and *SOX9* (with a $p < 0.05$) (Figure 5L).

To address the significance of these cancer-related genes in neuroblastoma, they were downregulated in NBAT1-sh cells using siRNAs (Figures S5F–S5H). As can be seen in Figure 5M, downregulation of *SOX9* and *OSMR*, but not *VCAN* affected the proliferation potential of the NBAT1-sh cells. Interestingly, downregulation of *VCAN*, *SOX9*, and *OSMR* also affected the invasive capacity of NBAT1-sh cells (Figure 5N). These results, taken together, suggest that higher expression of *SOX9*, *VCAN*, and *OSMR* may contribute to tumor progression in high-risk neuroblastoma patients.

To further understand the functional role of *NBAT-1* in tumor suppression and invasion, we have ectopically expressed *NBAT-1* in the neuroblastoma cell lines SK-N-AS and SK-N-BE(2), representing the two high-risk neuroblastoma subsets 11q- and MNA, respectively (Carén et al., 2010). *NBAT-1* overexpression resulted in decreased cell proliferation and invasion (Figures S5I–S5P), further corroborating its functional role in tumor progression. Interestingly, we observed consistent downregulation of *SOX9* and *VCAN* in both cell lines, indicating that *NBAT-1* may execute tumor suppression via repressing *SOX9* and *VCAN* genes.

We next sought to understand the mechanisms by which *NBAT-1* represses genes involved in tumor progression. To this end, RNA immunoprecipiation assay (RIP) demonstrated an interaction between *NBAT-1* and PRC2 complex member EZH2 (Figure 6A). To further understand the functional connection between *NBAT-1* and EZH2, total RNA from the *EZH2* downregulated SHSY-5Y cells was sequenced and investigated to see if there is any functional overlap between the expression changes seen in *EZH2* and *NBAT-1* downregulated cells (Table S7). These two data sets showed significant overlap ($r = 0.67$) (Figures 6B and 6C). Interestingly, a large majority of the overlapped genes were also enriched with H3K27me3 modification (Egan et al., 2013) (Figure 6C; Table S7). Genes implicated in cell proliferation and cell migration were upregulated in both *NBAT-1* and *EZH2* downregulated cells (Figures 5K, S5Q, and S5R). H3K27me3 modification at the promoters of some of these genes was analyzed upon *NBAT-1* downregulation using chromatin immunoprecipitation (ChIP)-qPCR (Figures 6D and 6E). Loss of H3K27me3 modification was observed at the promoter regions in NBAT-sh cells, indicating that the *NBAT-1*/EZH2 functional interaction suppresses its target genes implicated in cell proliferation and cell migration via chromatin level regulation.

Neuroblastoma Associated Transcript-1 Expression Is Critical for Neuronal Differentiation of Neuroblastoma Cells

As mentioned earlier in Figure 5H, neuronal processes are among the top biological processes that were perturbed upon

Figure 3. *Neuroblastoma Associated Transcript-1* Long Noncoding RNA as a Prognostic Marker for Neuroblastoma

(A) qRT-PCR showing differential expression of *NBAT-1* in 93 primary neuroblastoma tumors (cohort-I). The expression level of the RNA is presented after normalization to *GAPDH*. "*n*" represents the number of primary tumors used. The p value is presented as obtained from Welsh two sample t test (two-sided).

(B and C) RNA sequencing showing differential expression of *NBAT-1* in 498 tumors (cohort-II) in relation to risk groups and International Neuroblastoma Staging System stage. The p values were obtained from Mann-whitney (B) or Dunn's multiple comparison test (C).

(D–F) Kaplan-Meier curves indicating OS (D and E) and EFS (F) of patients in cohort-I and -II. The graphs depict p values as obtained from the Log-rank (Mantel-Cox) test. Numbers in bracket represent the number of patients in the respective groups.

(G) Waterfall plot of normalized log-transformed expression values of *NBAT-1* per survival status of the patient. Survival status of patients is presented in different colors (alive with disease [AWD], dead of disease [DOD], no evidence of disease [NED]).

(H) Multivariate Cox regression analysis investigating the independent prognostic value of *NBAT-1* expression with established prognostic markers in cohort-II.

For (A)–(C), values represent mean ±SD. *$p < 0.05$, **$p < 0.01$, and ***$p < 0.001$. See also Figure S3.

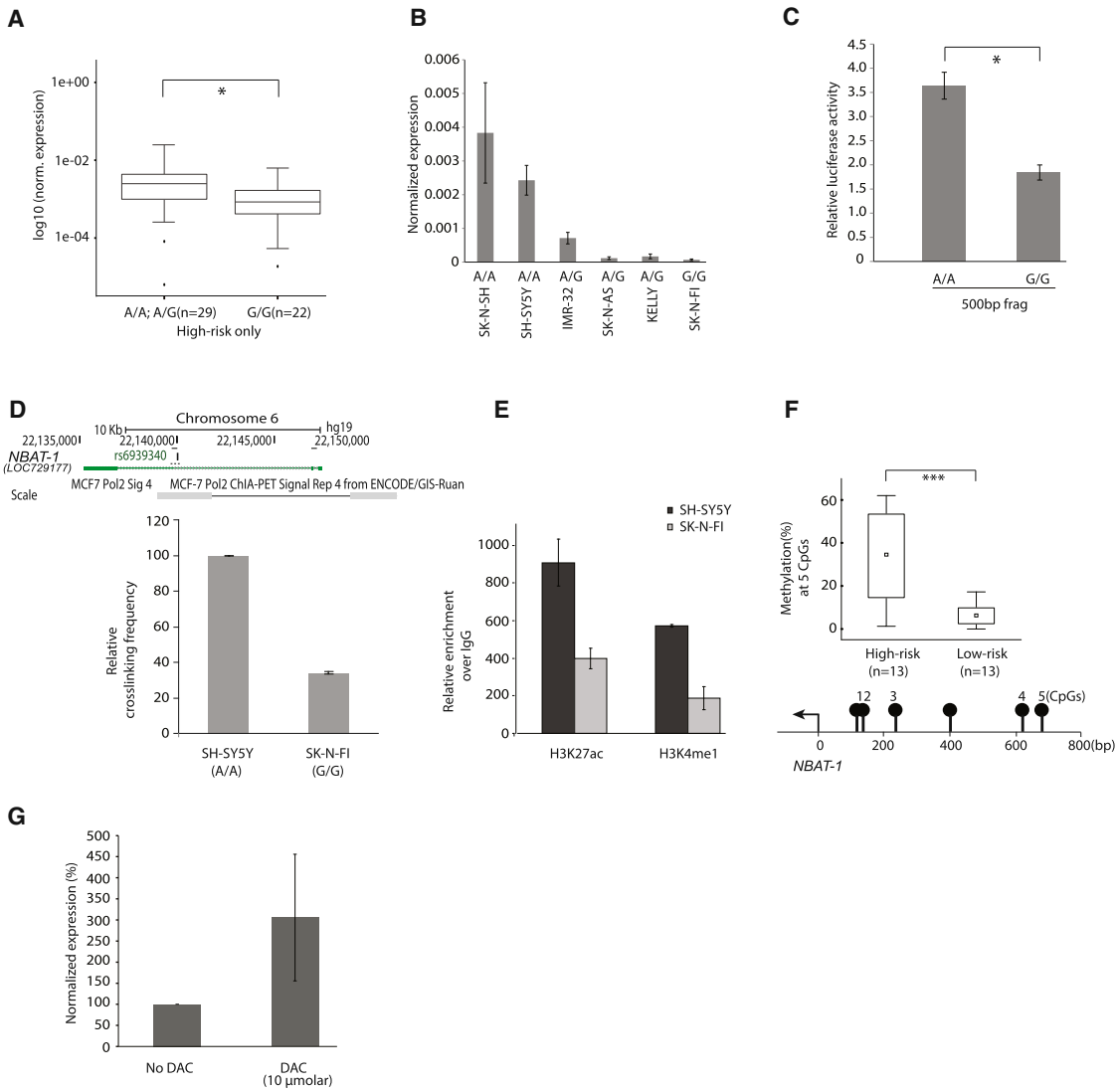

Figure 4. Risk Allele and DNA Methylation Contribute to *Neuroblastoma Associated Transcript-1* Differential Expression

(A) Differential expression of *NBAT-1* in high-risk tumors with A/A, A/G, or G/G genotype at the SNP: rs6939340. The *NBAT-1* expression was calculated as per Figure 3A.

(B) Allelic status at SNP: rs6939340 and *NBAT-1* expression in neuroblastoma cell lines.

(C) Relative luciferase activity of the transfected 500 bp fragments with A/A or G/G genotypes. The luciferase activity values are presented as enrichment over the pGL3 promoter vector luminescence values.

(D) Screenshot of the *NBAT-1* locus showing the position of the disease associated SNP, and ChIA-PET tags showing long range regulatory interactions between the SNP and *NBAT-1* promoter. Below the physical maps, the 3C experiment shows the relative cross-linking frequency between the *NBAT-1* promoter and the regulatory region containing the SNP in SH-SY5Y and SK-N-FI cell lines. Locations of the primers used in the 3C experiment are shown as solid black lines.

(E) ChIP was performed on the cell lines SH-SY5Y (with A/A genotype) and SK-N-FI (with G/G genotype) with antibodies to enhancer-specific histone marks H3K27ac and H3K4me1. The relative enrichment of the histone modifications are presented after normalizing to corresponding background immunoglobulin G (IgG) values from two independent biological experiments. The region where primers were designed for quantifying histone modifications is depicted as dashed line in Figure 4D.

(F) Average methylation (%) levels of the five analyzed CpGs in the *NBAT-1* upstream region analyzed by pyrosequencing. The boxplots represent methylation status in high-risk (n = 13) and low-risk (n = 13) neuroblastoma patients. Physical map depicts the CpGs chosen for methylation analysis and are marked as 1 to 5 in relation to transcription start site (TSS). The p value is presented as obtained from student's t test.

(G) Activation of *NBAT-1* upon DAC treatment of the SK-N-AS cell line with lower *NBAT-1* expression. *NBAT-1* expression levels in control and DAC treated cells were normalized to *GAPDH*. The data represents values obtained from three independent biological experiments.

For (A)–(G), values represent mean ±SD. *p < 0.05, **p < 0.01, and ***p < 0.001. See also Figure S4.

NBAT-1 knockdown. To investigate the functional role of *NBAT-1* in neuronal differentiation, we utilized SH-SY5Y cells' ability to differentiate into neurons upon retinoic acid (RA) treatment. Analysis of *NBAT-1* expression during the course of neuronal differentiation after the treatment of the SH-SY5Y cells with RA for up to 10 days revealed a significant increase in the

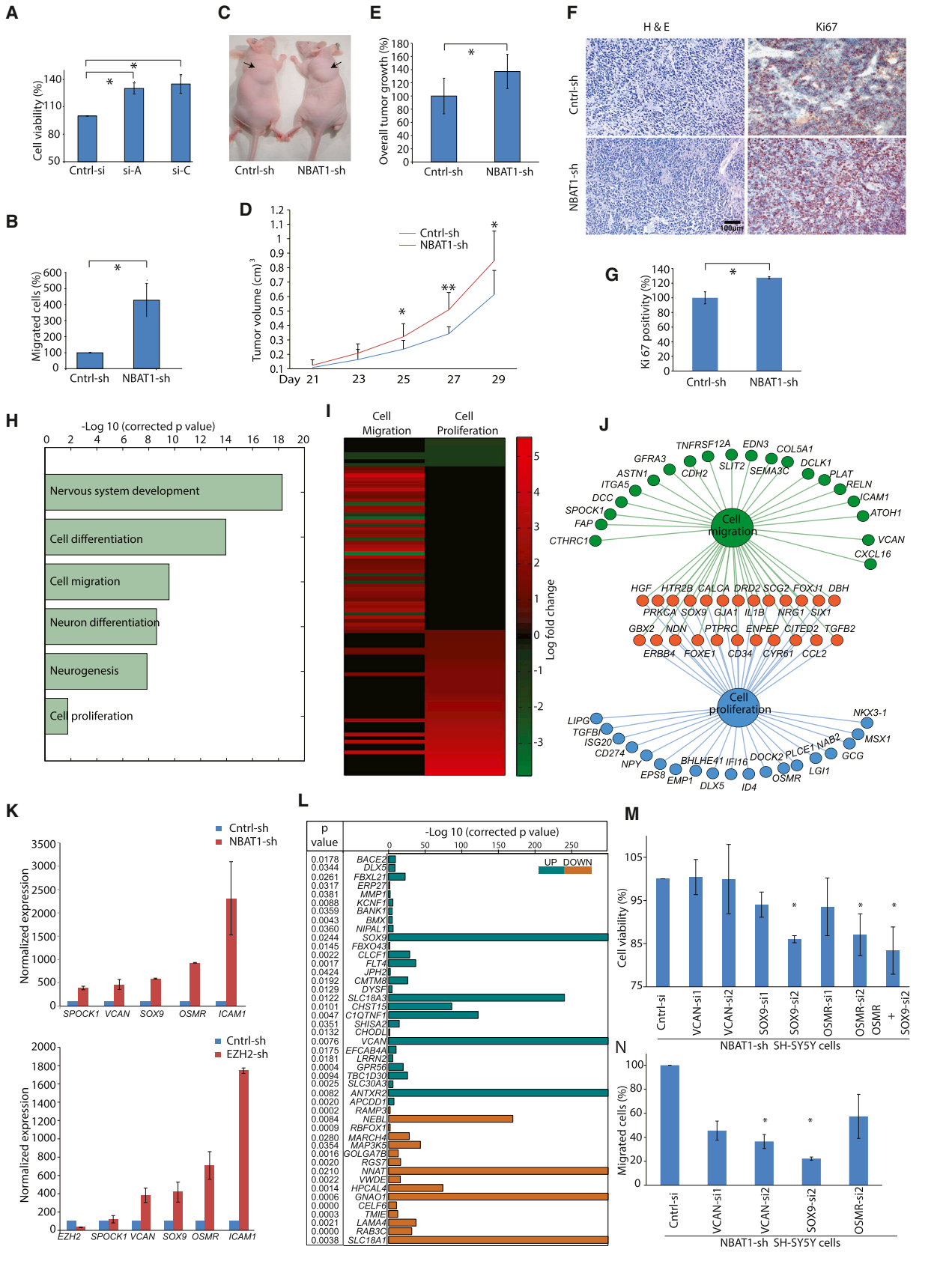

(legend on next page)

expression of *NBAT-1* (Figure 7A). Downregulation of *NBAT-1* in SH-SY5Y cells resulted in the impairment of the neuronal differentiation process, as these cells showed loss of expression of neuronal markers (*TH, TAU, MAPK*, and *NSE*) and impaired neurite outgrowth, a characteristic feature of neuronal differentiation (Figures 7A–7C and S6A–S6C). In order to gain further insights into the functional role of *NBAT-1* in the neuronal differentiation, total RNA from Cntrl-sh and NBAT1-sh cells, treated with RA for 0, 4, and 7 days, was sequenced. Expected expression patterns of known neuronal markers were found in the RA treated Cntrl-sh cells (Figures S6D–S6G). We observed 136 differentially expressed protein-coding genes between D0, D4, and D7 RA treated Cntrl-sh cells (Figure S6D), whereas in the case of RA treated NBAT1-sh cells, only 78 protein-coding genes were differentially expressed (2-fold; FDR < 0.05) (data not shown). Gene ontology (GO) analysis of the 136 genes from RA treated Cntrl-sh cells revealed enrichment of major neuronal processes such as neuronal differentiation, axonogenesis, neurogenesis, etc. No such significant enrichment of neuronal processes was found with NBAT1-sh cells (Figure 7D), again indicating that *NBAT-1* plays an important role in neuronal differentiation.

To obtain further insights into *NBAT-1* mediated neuronal differentiation, we chose to stably overexpress *NBAT-1* in the SK-N-AS and SK-N-BE(2) cell lines. *NBAT-1* overexpression induced neuronal differentiation of both cell lines, underscoring the importance of *NBAT-1* in neuronal differentiation (Figures S6H–S6O).

In order to identify genes/networks perturbed in the NBAT1-sh cells during RA induced neural differentiation, we have clustered the differentially expressed genes (1,956 genes) between Cntrl-sh and NBAT1-sh cells at D0, D4, and D7 (Figures 7E and 7F). The clustering resulted in five gene clusters with distinct expression patterns. Interestingly, the cluster IV genes (455 genes) with reduced expression levels at D4 and D7 showed significant enrichment for biological processes such as neuron differentiation, neurogenesis, axonogenesis, and nervous system development (Figure 7G; Table S8). We validated the expression of some of the key neuronal genes representing cluster IV using qRT-PCR (Figure 7H). We next investigated whether the *NBAT-1*/EZH2 functional interaction has any role in neuronal differentiation. Although a significant overlap was found between the cluster IV genes and the *EZH2* deregulated gene data set, there was a significant difference in the pattern of expression among the overlapped genes. In the *NBAT-1* gene data set, 63% of the overlapped genes show downregulation, whereas in the *EZH2* data set, 71% of the overlapped genes show increased expression (Figure S6P). More importantly, none of the cluster IV genes showed overlap with H3K27me3 ChIP followed by DNA sequencing (seq)-peaks. These observations indicate that *NBAT-1* and *EZH2* play critical roles in neurogenesis, but their functional interaction has no role in the regulation of neurogenesis.

We next sought to address the reasons underlying the downregulation of neuronal lineage-specific genes upon *NBAT-1* downregulation. A neuron restrictive silencing factor NRSF/REST, which represses the expression of neuronal genes in nonneuronal tissues and embryonic stem cells, was upregulated upon *NBAT-1* downregulation (Figures 8A and S7A). Also, an increased expression of *NRSF/REST* was found in MNA tumors relative to non-MNA tumors in the R2 data set (Figure S7B). Interestingly, a significant proportion of *NBAT-1* affected neuronal genes (cluster IV) have NRSF/REST binding sites, characterized in a publically available ChIP-seq data set (Figure 8B; Table S9) (Wang et al., 2012b), indicating that *NBAT-1* may control neural commitment via repressing the *NRSF/REST* pathway. Consistent with this notion, upregulation of several neuronal lineage-specific genes and restoration of the neuronal phenotype was observed when *NRSF/REST* was downregulated in the NBAT1-sh cells (Figures 8C, 8D, and S7C). It is also important to note that many REST targets such as *KLF7*, *SYT2*, and *PIPOX* are expressed at significantly lower levels in high-risk patients (Versteeg dataset from R2 database http://r2.amc.nl) (Figure S7D) and showed relaxation of their silencing upon *NRSF/REST* knockdown in the *NBAT-1* downregulated SH-SY5Y cells (Figure 8E). Collectively, these observations indicate that the regulation of key genes required for proper neuronal differentiation occurs via a *NBAT-1* regulated NRSF/REST pathway.

Figure 5. Downregulation of *Neuroblastoma Associated Transcript-1* Leads to Increased Cell Proliferation and Invasion

(A) (3-[4,5-dimethylthiazol-2-yl]-2,5 diphenyl tetrazolium bromide) (MTT) assay depicting the changes in viable cells post 48 hr siRNA knockdown of *NBAT-1* RNA with two siRNAs (si-A and si-C) and a nontarget control (Cntrl-si) in SH-SY5Y cells.

(B) Transwell Matrigel invasion assay showing percent increase in the invasion of the *NBAT-1* shRNA transduced cells (NBAT1-sh) compared to the cells transduced with control sh-RNA (Cntrl-sh).

(C–E) Subcutaneous injections were performed in nude mice to develop mouse xenografts with either Cntrl-sh (n = 9) or NBAT1-sh (n = 9) cells. (D) Injection of the *NBAT-1* depleted cells resulted in increase in tumor size up to 29 days. Representative picture (C) and graph (E) showing increased tumor volume in the mouse injected with NBAT1-sh cells, but not with Cntrl-sh cells.

(F) Representative sections of tumors stained with H&E and Ki67. Increased Ki67 immunostaining in NBAT1-sh xenografts is visible.

(G) Graph representing increased proliferative cells stained with Ki67 in NBAT1-sh xenografts as compared to Cntrl-sh.

(H) GO analysis of the differentially expressed protein coding genes between Cntrl-sh and NBAT1-sh cells.

(I) Heatmap showing changes in expression of genes involved in cell proliferation and cell migration in the *NBAT-1* downregulated cells as compared to the control cells.

(J) Gene network analysis using Cytoscape shows interactions of the differentially expressed genes (with 3-fold difference) implicated in cell proliferation and migration.

(K) qRT-PCR validation of some of the key genes implicated in cell proliferation and migration upon *NBAT-1* (upper panel) and *EZH2* downregulation (lower panel).

(L) Table shows the list of 45 genes (out of 1,348 differentially expressed genes between NBAT1-sh and Cntrl-sh cells), showing similar expression patterns between the R2 database; Versteeg dataset from R2 database (http://r2.amc.nl) (Molenaar et al., 2012) and the *NBAT-1* downregulated cells.

(M) MTT assay depicting the changes in viable cells post 48 hr of knockdown of *VCAN*, *SOX9*, or *OSMR* transcripts in NBAT1-sh cells using siRNAs.

(N) Transwell Matrigel invasion assay showing percent decrease in the invasion of the NBAT1-sh cells transfected with siRNAs against *VCAN*, *SOX9*, or *OSMR*.

For (A), (B), (D), (E), (G), (K), (M), and (N), values represent mean ±SD. *p < 0.05 and **p < 0.01. See also Figure S5 and Table S6.

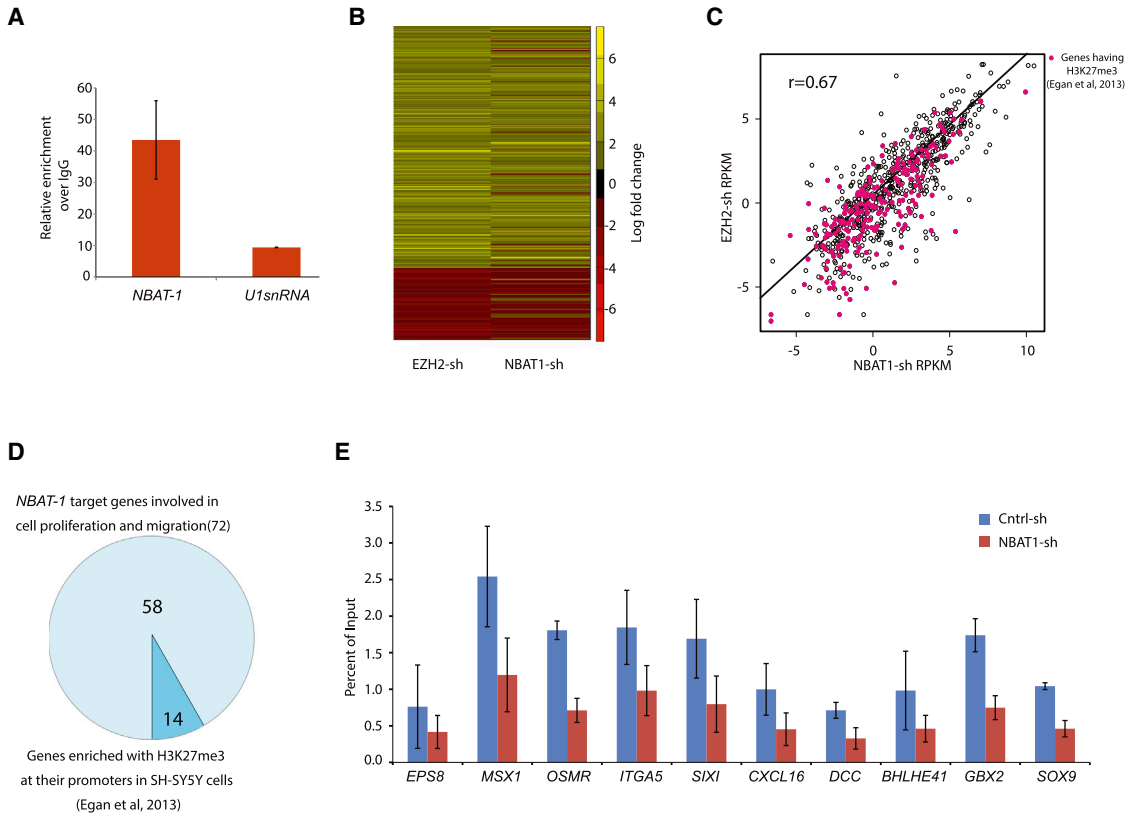

Figure 6. *Neuroblastoma Associated Transcript-1* Acts as a Tumor Suppressor via Interacting with EZH2

(A) RIP assay showing the interaction between *NBAT-1* RNA and EZH2. Graph shows the fold enrichment of EZH2 bound *NBAT-1* RNA over IgG. U1 snRNA enrichment was taken as negative control.

(B) Heatmap showing common expression changes upon downregulation of *NBAT-1* and *EZH2*.

(C) Scatter plot showing significant correlation between the expression changes in the *NBAT-1* and *EZH2* downregulated cells (Pearson correlation coefficient; r = 0.67). Genes enriched with H3K27me3 mark at their promoters (±3 kb from TSS) are highlighted (Egan et al., 2013).

(D) Pie chart showing the number of *NBAT-1*/EZH2 target genes implicated in cell proliferation and migration enriched with H3K27me3 marks.

(E) *NBAT-1*/EZH2 target genes showing changes in H2K27me3 levels upon *NBAT-1* downregulation as measured using ChIP assay. The relative enrichment of H3K27me3 over input at the target gene promoters is presented.

For (A) and (E), values represent mean ±SD. See also Table S7.

DISCUSSION

In this study, we characterized differentially expressed lncRNAs between low- and high-risk neuroblastomas. We identified 24 lncRNAs, which can distinguish the high-risk tumors from low-risk tumors. These noncoding signatures could serve as complementary information, alongside with established biomarkers such as amplification of the *MYCN* gene and heterozygous deletion of the 11q arm, for efficient stratification of the disease. In addition, this study also identified lncRNAs that map to commonly occurring nonrandom chromosome alterations, MNA, 1p deletion, and 11q deletion. LncRNAs that map to the amplicons on 2p associated with MNA and to the 11q deletion region could act as oncogene and tumor suppressor genes, respectively. Validation of their expression in an extended series of tumors suggests potential roles in the pathogenesis of MNA and 11q- tumors. Further characterization of the mode of action of these lncRNA would be needed to explain how their aberrant expression, due to genomic imbalances, might contribute to the pathogenesis of specific subtypes of the disease.

The current investigation implicates *NBAT-1* expression as an independent prognostic marker in patients with neuroblastoma. This RNA is expressed at lower levels in high-risk (both 11q- and MNA) tumors, and its lower expression could serve as a risk factor to predict adverse outcome among neuroblastoma patients. Our study suggests that multiple factors contribute to differential expression of *NBAT-1* among the neuroblastoma subtypes. Hypermethylation at the *NBAT-1* promoter in high-risk patients indicates that DNA methylation is one of the primary mechanisms that contribute to *NBAT-1* repression in these patients. In addition, we show that there is a functional correlation between *NBAT-1* expression and the previously identified high-risk associated SNP (rs6939340) on 6p22 in intron 2 of the *NBAT-1* gene (Maris et al., 2008). Thus, our study demonstrates that both genetic and epigenetic changes underlie the differential expression of *NBAT-1* in neuroblastoma subtypes.

Our cell culture and mouse xenograft models clearly demonstrate that *NBAT-1* has tumor suppressor properties, such as anticell proliferation and anticell invasion. In this context, detailed investigation of the *NBAT-1* target genes revealed an

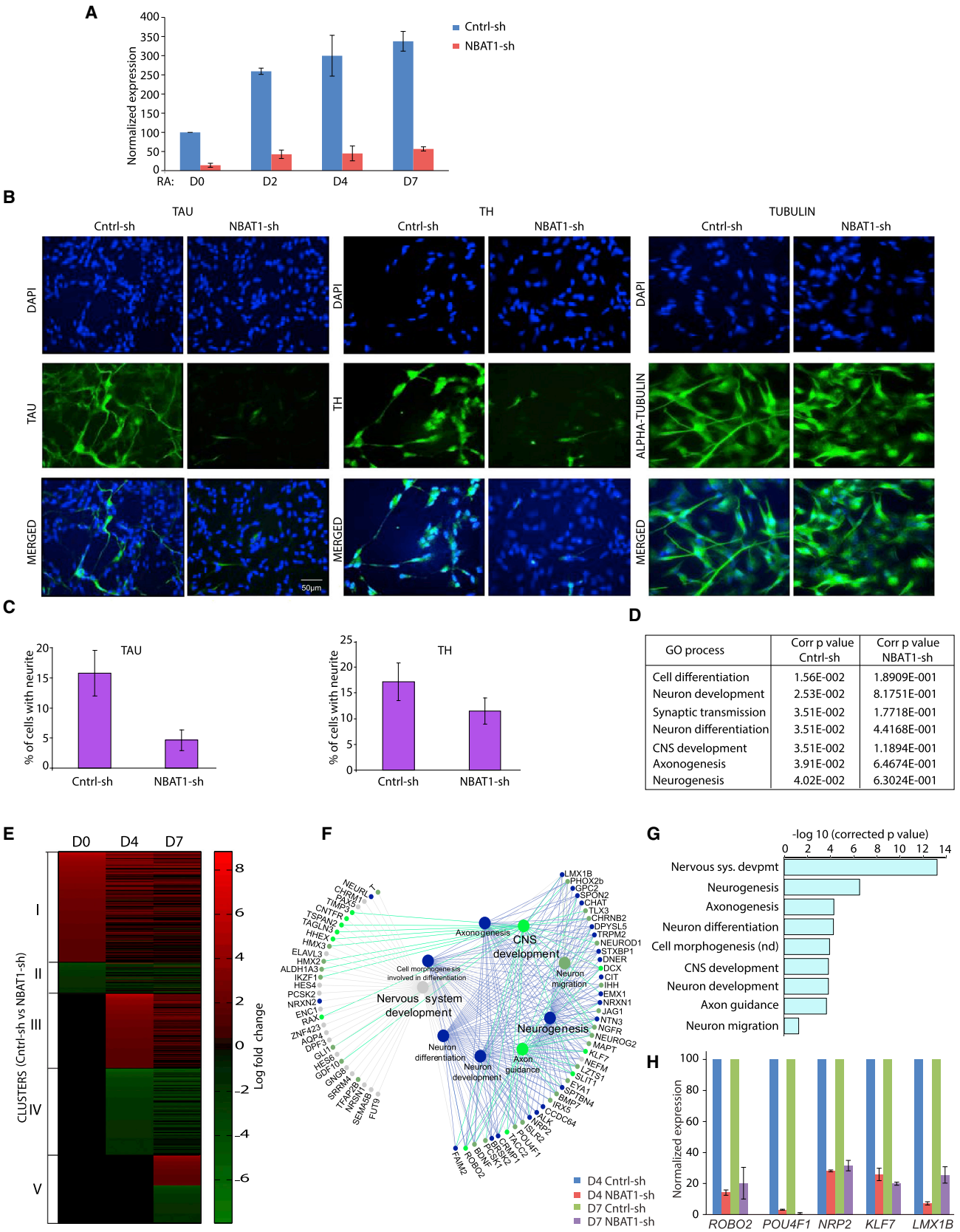

GO process	Corr p value Cntrl-sh	Corr p value NBAT1-sh
Cell differentiation	1.56E-002	1.8909E-001
Neuron development	2.53E-002	8.1751E-001
Synaptic transmission	3.51E-002	1.7718E-001
Neuron differentiation	3.51E-002	4.4168E-001
CNS development	3.51E-002	1.1894E-001
Axonogenesis	3.91E-002	6.4674E-001
Neurogenesis	4.02E-002	6.3024E-001

(legend on next page)

interconnected network of affected genes (Figure 5J). Some of the genes present in this network (*SOX9*, *VCAN*, and *OSMR)* have been shown to contribute to tumor progression in several cancer types. Loss of proliferative and invasive properties of NBAT1-sh cells upon downregulation of *SOX9*, *OSMR*, and *VCAN* indicates that *NBAT-1* controls tumor progression by suppressing these genes. The higher expression of *SOX9* and *VCAN* genes in high-risk tumors compared to low-risk neuroblastoma tumors in our and R2 data sets further supports their functional role in tumor progression in high-risk neuroblastomas. Importantly, *SOX9* maps to 17q24, and the gain of 17q is the most frequent abnormality in neuroblastoma tumors with poor prognosis (Carén et al., 2010; Lastowska et al., 2001). Collectively, these observations further emphasize the functional role of *SOX9* in neuroblastoma tumor progression.

Our data demonstrates that *NBAT-1* epigenetically controls the expression of target genes involved in cell proliferation and cell invasion by interacting with EZH2. Upregulation of *NBAT-1* target genes implicated in cell proliferation and invasion in both *EZH2* and *NBAT-1* knockdown cells and loss of H3K27me3 from their promoter regions, suggest that a *NBAT-1*/EZH2 functional interaction may repress these genes in low-risk patients via chromatin level regulation. The decreased *NBAT-1* expression in high-risk tumors could be the underlying cause for the increased cell proliferation and cell invasion in these tumors by activating *SOX9* and *VCAN* dependent pathways. However, increased *EZH2* expression has been observed in high-risk neuroblastoma tumors, and this has been functionally linked to increased cell proliferation (Wang et al., 2012a). Considering that *NBAT-1* is expressed at low level in high-risk tumors, we are tempted to speculate that *NBAT-1* acts as a scaffold for the EZH2 recruitment, and that EZH2 is no longer recruited to repress *NBAT-1*/EZH2 target genes in the absence of *NBAT-1* expression, thus increasing the expression of genes involved in tumor progression (Figure 8F). Consistent with this idea, overexpression of *EZH2* in NBAT1-sh cells had no significant effect on the expression of *SOX9*, *OSMR*, and *VCAN* genes (data not shown).

Another interesting aspect of the current study is *NBAT-1*'s functional role in RA induced neuronal differentiation. Impaired neuronal differentiation of neuronal precursor cells is one of the characteristic features of high-risk neuroblastomas (Nakagawara et al., 1993). We demonstrate that the inability of NBAT1-sh cells to achieve neuronal differentiation is due to upregulation of the NRSF/REST pathway and consequent downregulation of some of its key neuronal-specific genes (Figure 8F). Furthermore, the restoration of neuronal phenotype and relaxation of silencing of some of the key neuronal-specific genes upon *NRSF/REST* downregulation in the NBAT1-sh cells, suggests that *NBAT-1* controls the neuronal lineage commitment via regulating *NRSF/REST* activity. Increased expression of *NRSF/REST* in MNA tumors relative to non-MNA tumors in the Versteeg dataset from R2 database (http://r2.amc.nl), and the recent suggestion that *HOXC9* induced regression of neuroblastoma tumors involves downregulation of *NRSF/REST* (Kocak et al., 2013) provides an explanation for the impairment of differentiation of neuronal precursor cells in high-risk patients. In addition, upregulation of *NRSF/REST* in medulloblastoma patients has also been shown to affect the differentiation of neural stem/progenitors into neurons (Su et al., 2006). These observations clearly indicate that *NBAT-1* mediated NRSF/REST suppression could be a critical pathway regulating the neuronal fate commitment. Disturbance in this pathway could be one of the underlying causes for neural related cancers that are a result of impairment of neuronal differentiation. The RNA-sequencing data of *NBAT-1* and *EZH2* downregulated cells indicate that the *NBAT-1*/EZH2 functional interaction does not have any functional role in the neural lineage commitment. Though *EZH2* and *NBAT-1* have critical roles in neurogenesis, they operate by different pathways, and this observation is consistent with the fact that downregulation of *EZH2* promotes neurogenesis (Wang et al., 2012a), while that of *NBAT-1* impairs neuronal differentiation.

Taken together, these observations reveal that *NBAT-1* is a biomarker for risk assessment for neuroblastoma tumors. Additionally, the role of *NBAT-1* in cell proliferation, invasion, and neuronal differentiation elucidates mechanisms and gene networks involved in neuroblastoma tumor development and progression. Both *NBAT-1* and its downstream effectors (*SOX9* and *NRSF/REST*) could serve as potential targets for drug development and options for neuroblastoma clinical treatment.

EXPERIMENTAL PROCEDURES

Patient and Tumor Material

Neuroblastoma primary tumors were obtained at surgery, snap frozen, and stored at −70°C until analysis. For RNA sequencing, a set of 15 tumors were selected: three clinical low-risk (Cohn et al., 2009) with a numerical only genotype (Carén et al., 2010), and 12 high-risk tumors with MYCN-amplification (n = 6) and 11q deletion (n = 6). In cohort I, a total of 106 Swedish and two German patients were included according to ethical permit number (Dnr 2011/354), it was approved by Regional Ethical Review Board, Uppsala University, Uppsala, and informed consent from the legal guardian was secured. In cohort II, RNA-seq data from 498 patients was used. These patients were

Figure 7. *Neuroblastoma Associated Transcript-1* Expression Is Critical for Neuronal Differentiation

(A) qRT-PCR measurement of *NBAT-1* expression during RA induced neuronal differentiation of the SH-SY5Y cells transduced with Cntrl-sh and NBAT1-sh lentiviral particles.

(B) Immunostaining of the Cntrl-sh and NBAT1-sh SH-SY5Y cells 5 days after RA treatment using the antibodies specific to neuronal markers TAU and TH. TUBULIN immunostaining is used as a control.

(C) Percent of neurite outgrowths observed in the Cntrl-sh and NBAT1-sh cells stained with TAU and TH.

(D) GO analysis of the differentially expressed genes in the Cntrl-sh *(136 genes)* or NBAT1-sh *(78 genes)* cells treated with RA for 0, 4, and 7 days.

(E) Heatmap showing clustering of all genes that displayed a 3-fold or greater difference in expression levels between *NBAT-1* depleted SH-SY5Y cells and Cntrl-sh cells at days 0, 4, and 7 of RA treatment. Cluster IV genes were not induced during differentiation, upon loss of *NBAT-1*.

(F) Network analysis on the cluster IV genes generated using Cytoscape.

(G) GO analysis of the cluster IV revealed enrichment of biological processes related to neuronal development and differentiation. nd, neuronal differentiation.

(H) qRT-PCR validation of some of the cluster IV genes in the NBAT1-sh cells post RA induced differentiation.

For (A), (C), and (H), values represent mean ±SD. See also Figure S6 and Table S8.

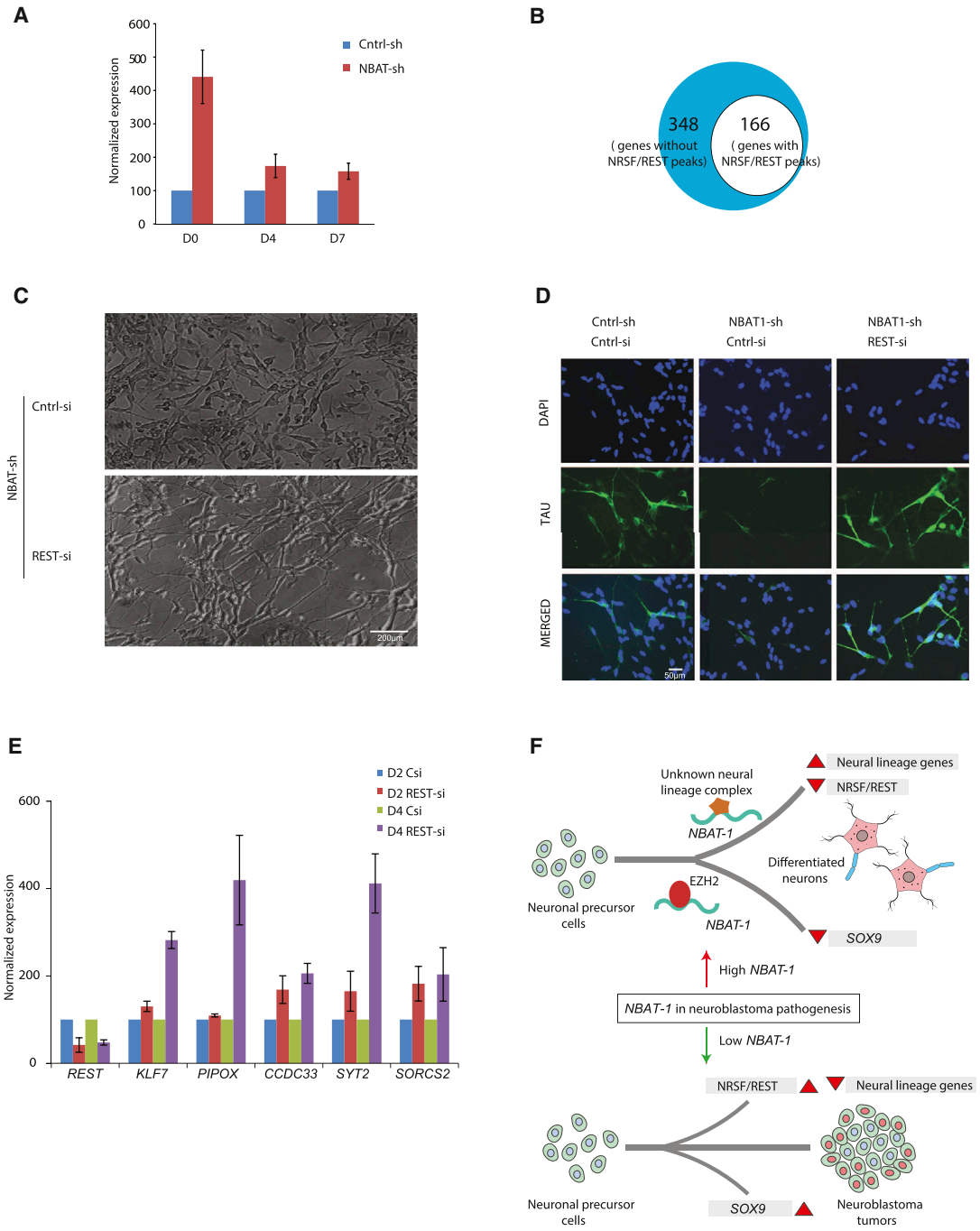

Figure 8. *Neuroblastoma Associated Transcript-1* Regulates Neural Lineage Commitment through the Suppression of NRSF/REST

(A) qRT-PCR measurement of *NRSF/REST* expression during RA induced differentiation of NBAT1-sh and Cntrl-sh cells.

(B) Venn-diagram showing number of cluster IV genes (Figures 7E and 7F) with NRSF/REST binding sites (Wang et al., 2012b).

(C) *NRSF/REST* downregulation rescues neuronal phenotype in NBAT1-sh cells. Bright field microscopy images (20×) of SH-SY5Y (NBAT1-sh) cells, transfected with *REST* siRNA (REST-si) or Cntrl siRNA (Cntrl-si) followed by 4 days of RA treatment.

(D) Immunostaining of the Cntrl-sh and NBAT1-sh cells, treated with Cntrl-si or REST-si followed by 4 days of RA treatment, using the antibodies specific to neuronal marker *TAU*.

(E) qRT-PCR measurement of relaxation of NRSF/REST target genes upon downregulation of *REST* in the NBAT1-sh cells.

(F) Model explaining the tumor suppressor and neuronal differentiation properties of *NBAT-1*. *NBAT-1* functional interaction with EZH2, a member of PRC2 complex, controls tumor progression by suppressing protumor genes such as *SOX9*, *VCAN*, and *OSMR* via regulating chromatin structure. On the other hand, *NBAT-1* promotes neuronal lineage commitment by suppressing *NRSF/REST* by interacting with an unknown neuronal-linage-specific transcriptional repressor. The *NBAT-1*/EZH2 interaction has no functional role in the repression of *NRSF/REST*.

For (A) and (E), values represent mean ±SD. See also Figure S7 and Table S9.

registered in respective clinical trials with informed consent (NB2004, 04-049; NB97, 9764; ethical committee of the Medical Faculty of the University of Cologne). Details of two tumor cohorts, Array-CGH profiles of the sequenced tumors, and other experimental procedures are described in detail in Supplemental Experimental Procedures.

Mouse Xenograft Tumor Model and Histology

3×10^6 cells infected with either Cntrl-sh or NBAT1-sh (n = 9) were subcutaneously injected on the dorsal back region of 5- to 6-week-old Bagg Albino (inbred research mouse strain) nude male mice (Charles River Laboratories) as described earlier (Nallapalli et al., 2012). Tumors were harvested and half of each tumor was frozen in liquid nitrogen and stored in −80°C, whereas the other half was fixed in 4% paraformaldehyde for immunostaining. All the mouse experiments were approved by Animal Ethical Review Board, University of Gothenburg, Gothenburg, Sweden (Ethical permit number-62/14). Paraffin-embedded tumor tissues were analyzed by hematoxylin and eosin staining (H&E). Immunostaining with Ki67 (Thermo Scientific) antibody was performed to detect the number of replicating cells as described earlier (Nallapalli et al., 2012). Ki67 staining positivity was quantified in three different high power fields of each section, and the mean ±SD values were given.

RNA Isolation and Library Preparation

Tumors from neuroblastoma patients were cut on dry ice. Total RNA was isolated from the tumors using the Promega Total RNA Isolation Kit (Promega). Isolated RNA was ribo-depleted using the Ribominus Eukaryotic Kit (Invitrogen) according to the manufacturer's instructions. Ribo-depleted RNA was used to prepare a whole transcriptome library (Applied Biosystems) as per the manufacturer's protocol. Quality, size, and concentration of the RNA during library preparation were analyzed using Bioanalyser 2100 (RNA Pico Kit, Agilent). Final amplified cDNA library was analyzed using DNA Hypersensitive Kit (Agilent).

Pyrosequencing

Pyrosequencing was performed to analyze the methylation levels at five CpGs sites (labeled in Figure 4F) at the *NBAT-1* promoter. Genomic DNA from 13 tumors, each representing low-risk and high-risk tumors, were bisulphite converted and analyzed as described earlier (Martinelli et al., 2013). The primers used for pyrosequencing analysis are mentioned in the Supplemental Experimental Procedures.

ACCESSION NUMBERS

The RNA sequencing files (FASTQ) have been deposited in European Nucleotide Archive (ENA) with study accession number: PRJEB6912 (http://www.ebi.ac.uk/ena/data/view/PRJEB6912).

SUPPLEMENTAL INFORMATION

Supplemental Information includes Supplemental Experimental Procedures, seven figures, and nine tables and can be found with this article online at http://dx.doi.org/10.1016/j.ccell.2014.09.014.

AUTHOR CONTRIBUTIONS

G.K.P., S.M., and C.K. conceived and designed the experiments. G.K.P. and S.M. performed the experiments. S.S. performed bioinformatics analysis. Cohort II validations were done by F.H. M.K. performed pyrosequencing and analyzed data. K.M. performed ChIP and luciferase assays. S.F. performed somatic mutational analysis. A.G. performed cell line expression analysis. T.M. performed 3C experiments. E.L. provided *NBAT-1* conservation and bodymap2 data. S.B. and L.M.A. performed xenograft experiments. M.O. performed statistical analysis. J.A. and S.P. provided reagents. G.K.P., M.F., T.M., F.H., P.K., and C.K. analyzed data and wrote the paper. G.K.P. and S.M. share equal authorship.

ACKNOWLEDGMENTS

This work was supported by grants from the Swedish Cancer Research foundation (Cancerfonden: Kontrakt no. 13 0531), Swedish Research Council (VR-M: K2014-67X-20781-07-4), Barncancerfonden (PR2013-0048), and Läkar Utbildnings Avtalet/Avtalet om Läkarutbildning och medicinsk Forskning to C.K. The authors would like to thank Danielle and Jean Thierry-Mieg (NIH/National Center for Biotechnology Information, Bethesda) for their data analysis using the Magic-AceView pipeline, as well as Frederik Roels and Ruth Volland (University Children's Hospital Cologne) for statistical support. We thank Professor Lars Gunnar Larsson, Karolinska Institute, for providing neuroblastoma cell lines and SciLifeLab, Uppsala, for RNA sequencing.

Received: November 14, 2013
Revised: April 8, 2014
Accepted: September 25, 2014
Published: November 10, 2014

REFERENCES

Batista, P.J., and Chang, H.Y. (2013). Long noncoding RNAs: cellular address codes in development and disease. Cell *152*, 1298–1307.

Brodeur, G.M., Seeger, R.C., Schwab, M., Varmus, H.E., and Bishop, J.M. (1984). Amplification of N-myc in untreated human neuroblastomas correlates with advanced disease stage. Science *224*, 1121–1124.

Brodeur, G.M. (2003). Neuroblastoma: biological insights into a clinical enigma. Nat. Rev. Cancer *3*, 203–216.

Carén, H., Abel, F., Kogner, P., and Martinsson, T. (2008a). High incidence of DNA mutations and gene amplifications of the ALK gene in advanced sporadic neuroblastoma tumours. Biochem. J. *416*, 153–159.

Carén, H., Erichsen, J., Olsson, L., Enerbäck, C., Sjöberg, R.M., Abrahamsson, J., Kogner, P., and Martinsson, T. (2008b). High-resolution array copy number analyses for detection of deletion, gain, amplification and copy-neutral LOH in primary neuroblastoma tumors: four cases of homozygous deletions of the CDKN2A gene. BMC Genomics *9*, 353.

Carén, H., Kryh, H., Nethander, M., Sjöberg, R.M., Träger, C., Nilsson, S., Abrahamsson, J., Kogner, P., and Martinsson, T. (2010). High-risk neuroblastoma tumors with 11q-deletion display a poor prognostic, chromosome instability phenotype with later onset. Proc. Natl. Acad. Sci. USA *107*, 4323–4328.

Caron, H. (1995). Allelic loss of chromosome 1 and additional chromosome 17 material are both unfavourable prognostic markers in neuroblastoma. Med. Pediatr. Oncol. *24*, 215–221.

Chen, Y., Takita, J., Choi, Y.L., Kato, M., Ohira, M., Sanada, M., Wang, L., Soda, M., Kikuchi, A., Igarashi, T., et al. (2008). Oncogenic mutations of ALK kinase in neuroblastoma. Nature *455*, 971–974.

Cheon, D.J., Tong, Y., Sim, M.S., Dering, J., Berel, D., Cui, X., Lester, J., Beach, J.A., Tighiouart, M., Walts, A.E., et al. (2014). A collagen-remodeling gene signature regulated by TGF-β signaling is associated with metastasis and poor survival in serous ovarian cancer. Clin. Cancer Res. *20*, 711–723.

Cohn, S.L., Pearson, A.D., London, W.B., Monclair, T., Ambros, P.F., Brodeur, G.M., Faldum, A., Hero, B., Iehara, T., Machin, D., et al.; INRG Task Force (2009). The International Neuroblastoma Risk Group (INRG) classification system: an INRG Task Force report. J. Clin. Oncol. *27*, 289–297.

Diskin, S.J., Capasso, M., Schnepp, R.W., Cole, K.A., Attiyeh, E.F., Hou, C., Diamond, M., Carpenter, E.L., Winter, C., Lee, H., et al. (2012). Common variation at 6q16 within HACE1 and LIN28B influences susceptibility to neuroblastoma. Nat. Genet. *44*, 1126–1130.

Egan, C.M., Nyman, U., Skotte, J., Streubel, G., Turner, S., O'Connell, D.J., Rraklli, V., Dolan, M.J., Chadderton, N., Hansen, K., et al. (2013). CHD5 is required for neurogenesis and has a dual role in facilitating gene expression and polycomb gene repression. Dev. Cell *26*, 223–236.

Fischer, M., Spitz, R., Oberthür, A., Westermann, F., and Berthold, F. (2008). Risk estimation of neuroblastoma patients using molecular markers. Klin. Padiatr. *220*, 137–146.

George, R.E., Sanda, T., Hanna, M., Fröhling, S., Luther, W., 2nd, Zhang, J., Ahn, Y., Zhou, W., London, W.B., McGrady, P., et al. (2008). Activating mutations in ALK provide a therapeutic target in neuroblastoma. Nature *455*, 975–978.

Guo, C., White, P.S., Weiss, M.J., Hogarty, M.D., Thompson, P.M., Stram, D.O., Gerbing, R., Matthay, K.K., Seeger, R.C., Brodeur, G.M., and Maris, J.M. (1999). Allelic deletion at 11q23 is common in MYCN single copy neuroblastomas. Oncogene *18*, 4948–4957.

Janoueix-Lerosey, I., Lequin, D., Brugières, L., Ribeiro, A., de Pontual, L., Combaret, V., Raynal, V., Puisieux, A., Schleiermacher, G., Pierron, G., et al. (2008). Somatic and germline activating mutations of the ALK kinase receptor in neuroblastoma. Nature *455*, 967–970.

Kamijo, T., and Nakagawara, A. (2012). Molecular and genetic bases of neuroblastoma. Int. J. Clin. Oncol. *17*, 190–195.

Kanduri, C. (2011). Long noncoding RNA and epigenomics. Adv. Exp. Med. Biol. *722*, 174–195.

Kocak, H., Ackermann, S., Hero, B., Kahlert, Y., Oberthuer, A., Juraeva, D., Roels, F., Theissen, J., Westermann, F., Deubzer, H., et al. (2013). Hox-C9 activates the intrinsic pathway of apoptosis and is associated with spontaneous regression in neuroblastoma. Cell Death Dis. *4*, e586.

Kopp, J.L., von Figura, G., Mayes, E., Liu, F.F., Dubois, C.L., Morris, J.P., 4th, Pan, F.C., Akiyama, H., Wright, C.V., Jensen, K., et al. (2012). Identification of Sox9-dependent acinar-to-ductal reprogramming as the principal mechanism for initiation of pancreatic ductal adenocarcinoma. Cancer Cell *22*, 737–750.

Lastowska, M., Cullinane, C., Variend, S., Cotterill, S., Bown, N., O'Neill, S., Mazzocco, K., Roberts, P., Nicholson, J., Ellershaw, C., et al.; United Kingdom Children Cancer Study Group and the United Kingdom Cancer Cytogenetics Group (2001). Comprehensive genetic and histopathologic study reveals three types of neuroblastoma tumors. J. Clin. Oncol. *19*, 3080–3090.

Lawrence, M.S., Stojanov, P., Polak, P., Kryukov, G.V., Cibulskis, K., Sivachenko, A., Carter, S.L., Stewart, C., Mermel, C.H., Roberts, S.A., et al. (2013). Mutational heterogeneity in cancer and the search for new cancer-associated genes. Nature *499*, 214–218.

Li, G., Ruan, X., Auerbach, R.K., Sandhu, K.S., Zheng, M., Wang, P., Poh, H.M., Goh, Y., Lim, J., Zhang, J., et al. (2012). Extensive promoter-centered chromatin interactions provide a topological basis for transcription regulation. Cell *148*, 84–98.

Maris, J.M., Mosse, Y.P., Bradfield, J.P., Hou, C., Monni, S., Scott, R.H., Asgharzadeh, S., Attiyeh, E.F., Diskin, S.J., Laudenslager, M., et al. (2008). Chromosome 6p22 locus associated with clinically aggressive neuroblastoma. N. Engl. J. Med. *358*, 2585–2593.

Martinelli, S., Kanduri, M., Maffei, R., Fiorcari, S., Bulgarelli, J., Marasca, R., and Rosenquist, R. (2013). ANGPT2 promoter methylation is strongly associated with gene expression and prognosis in chronic lymphocytic leukemia. Epigenetics: official journal of the DNA Methylation Society *8*, 720–729.

Matheu, A., Collado, M., Wise, C., Manterola, L., Cekaite, L., Tye, A.J., Canamero, M., Bujanda, L., Schedl, A., Cheah, K.S., et al. (2012). Oncogenicity of the developmental transcription factor Sox9. Cancer Res. *72*, 1301–1315.

Molenaar, J.J., Koster, J., Zwijnenburg, D.A., van Sluis, P., Valentijn, L.J., van der Ploeg, I., Hamdi, M., van Nes, J., Westerman, B.A., van Arkel, J., et al. (2012). Sequencing of neuroblastoma identifies chromothripsis and defects in neuritogenesis genes. Nature *483*, 589–593.

Monclair, T., Brodeur, G.M., Ambros, P.F., Brisse, H.J., Cecchetto, G., Holmes, K., Kaneko, M., London, W.B., Matthay, K.K., Nuchtern, J.G., et al.; INRG Task Force (2009). The International Neuroblastoma Risk Group (INRG) staging system: an INRG Task Force report. J. Clin. Oncol. *27*, 298–303.

Mossé, Y.P., Laudenslager, M., Longo, L., Cole, K.A., Wood, A., Attiyeh, E.F., Laquaglia, M.J., Sennett, R., Lynch, J.E., Perri, P., et al. (2008). Identification of ALK as a major familial neuroblastoma predisposition gene. Nature *455*, 930–935.

Nakagawara, A., Arima-Nakagawara, M., Scavarda, N.J., Azar, C.G., Cantor, A.B., and Brodeur, G.M. (1993). Association between high levels of expression of the TRK gene and favorable outcome in human neuroblastoma. N. Engl. J. Med. *328*, 847–854.

Nallapalli, R.K., Ibrahim, M.X., Zhou, A.X., Bandaru, S., Sunkara, S.N., Redfors, B., Pazooki, D., Zhang, Y., Borén, J., Cao, Y., et al. (2012). Targeting filamin A reduces K-RAS-induced lung adenocarcinomas and endothelial response to tumor growth in mice. Mol. Cancer *11*, 50.

Pollard, K.S., Hubisz, M.J., Rosenbloom, K.R., and Siepel, A. (2010). Detection of nonneutral substitution rates on mammalian phylogenies. Genome Res. *20*, 110–121.

Prensner, J.R., and Chinnaiyan, A.M. (2011). The emergence of lncRNAs in cancer biology. Cancer Discov *1*, 391–407.

Prensner, J.R., Iyer, M.K., Balbin, O.A., Dhanasekaran, S.M., Cao, Q., Brenner, J.C., Laxman, B., Asangani, I.A., Grasso, C.S., Kominsky, H.D., et al. (2011). Transcriptome sequencing across a prostate cancer cohort identifies PCAT-1, an unannotated lincRNA implicated in disease progression. Nat. Biotechnol. *29*, 742–749.

Pugh, T.J., Morozova, O., Attiyeh, E.F., Asgharzadeh, S., Wei, J.S., Auclair, D., Carter, S.L., Cibulskis, K., Hanna, M., Kiezun, A., et al. (2013). The genetic landscape of high-risk neuroblastoma. Nat. Genet. *45*, 279–284.

Sausen, M., Leary, R.J., Jones, S., Wu, J., Reynolds, C.P., Liu, X., Blackford, A., Parmigiani, G., Diaz, L.A., Jr., Papadopoulos, N., et al. (2013). Integrated genomic analyses identify ARID1A and ARID1B alterations in the childhood cancer neuroblastoma. Nat. Genet. *45*, 12–17.

Schwab, M. (1998). Amplification of oncogenes in human cancer cells. BioEssays *20*, 473–479.

Spitz, R., Hero, B., Ernestus, K., and Berthold, F. (2003). Deletions in chromosome arms 3p and 11q are new prognostic markers in localized and 4s neuroblastoma. Clin. Cancer Res. *9*, 52–58.

Spizzo, R., Almeida, M.I., Colombatti, A., and Calin, G.A. (2012). Long non-coding RNAs and cancer: a new frontier of translational research? Oncogene *31*, 4577–4587.

Su, X., Gopalakrishnan, V., Stearns, D., Aldape, K., Lang, F.F., Fuller, G., Snyder, E., Eberhart, C.G., and Majumder, S. (2006). Abnormal expression of REST/NRSF and Myc in neural stem/progenitor cells causes cerebellar tumors by blocking neuronal differentiation. Mol. Cell. Biol. *26*, 1666–1678.

Taft, R.J., Pang, K.C., Mercer, T.R., Dinger, M., and Mattick, J.S. (2010). Non-coding RNAs: regulators of disease. J. Pathol. *220*, 126–139.

Wang, C., Liu, Z., Woo, C.W., Li, Z., Wang, L., Wei, J.S., Marquez, V.E., Bates, S.E., Jin, Q., Khan, J., et al. (2012a). EZH2 Mediates epigenetic silencing of neuroblastoma suppressor genes CASZ1, CLU, RUNX3, and NGFR. Cancer Res. *72*, 315–324.

Wang, J., Zhuang, J., Iyer, S., Lin, X., Whitfield, T.W., Greven, M.C., Pierce, B.G., Dong, X., Kundaje, A., Cheng, Y., et al. (2012b). Sequence features and chromatin structure around the genomic regions bound by 119 human transcription factors. Genome Res. *22*, 1798–1812.

Wang, L., Park, H.J., Dasari, S., Wang, S., Kocher, J.P., and Li, W. (2013). CPAT: Coding-Potential Assessment Tool using an alignment-free logistic regression model. Nucleic Acids Res. *41*, e74.

West, N.R., Murphy, L.C., and Watson, P.H. (2012). Oncostatin M suppresses oestrogen receptor-α expression and is associated with poor outcome in human breast cancer. Endocr. Relat. Cancer *19*, 181–195.

Whitehead, J., Pandey, G.K., and Kanduri, C. (2009). Regulation of the mammalian epigenome by long noncoding RNAs. Biochim. Biophys. Acta *1790*, 936–947.

Yeung, T.L., Leung, C.S., Wong, K.K., Samimi, G., Thompson, M.S., Liu, J., Zaid, T.M., Ghosh, S., Birrer, M.J., and Mok, S.C. (2013). TGF-β modulates ovarian cancer invasion by upregulating CAF-derived versican in the tumor microenvironment. Cancer Res. *73*, 5016–5028.